Source model of the great 2011 Tohoku earthquake estimated from tsunami waveforms and crustal deformation data

Aditya Riadi Gusman[1], Yuichiro Tanioka[1], Shinichi Sakai[2], and Hiroaki Tsushima[3].

[1)] Institute of Seismology and Volcanology, Hokkaido University

[2)] Earthquake Research Institute, University of Tokyo

[3)] Meteorological Research Institute, Japan Meteorological Agency

Abstract

The slip distribution of the 11 March 2011 Tohoku earthquake is inferred from tsunami waveforms, GPS data, and seafloor crustal deformation data. The major slip region extends all the way to the trench, and the large slip area extends 300 km long and 160 km wide. The largest slip of 44 m is located up-dip of the hypocenter. The large slip amount, about 41 m, ruptured the plate interface near the trench. The seismic moment calculated from the estimated slip distribution is 5.5×10^{22} N m (Mw 9.1). The large tsunami due to the 2011 Tohoku earthquake is generated from those large slip areas near the trench. The additional uplift at the sedimentary wedge as suggested for the 1896 Sanriku earthquake may have occurred during the 2011 Tohoku earthquake, too.

Keywords: tsunami waveforms, GPS data, seafloor crustal deformation data, the 2011 Tohoku earthquake

1. Introduction

The great 2011 Tohoku earthquake occurred on 11 March 2011 at 5:46:18 UTC with epicenter at 38.104° N and 142.861° E off the east coast of Tohoku and about 130 km from Sendai, Japan, according to the Japan Meteorological Agency (JMA). The largest foreshock

occurred at 2:45:13 UTC on 9 March 2011 with Mw 7.3 (JMA) at 38.328° N and 143.28° E. The largest aftershock with Mw 7.7 occurred approximately 28 min after the mainshock (6:15:34 UTC) at 36.108° N and 141.265° E (JMA). Approximately 39 min after the mainshock (6:25:44 UTC) a large extensional faulting (Mw 7.5) occurred in the outer-rise at 37.837° N and 144.894° E (JMA). **Fig. 1** is a map showing the location of the mainshock, foreshocks and aftershocks.

The Global Centroid Moment Tensor (GCMT) solution estimated that the 2011 Tohoku earthquake released seismic moment of 5.3×10^{22} N m (Mw 9.1). The dip angle at the centroid is ranging from 10° to 14° (GCMT, WCMT, and USGS). Seismic reflection and refraction images suggest that the dip angle near the trench is about 3° (Tsuji et al., 2011; Ito et al., 2011). A rupture model of the 2011 earthquake by Ammon et al. (2011) included a low initial rupture speed (1.5 km/s) near the hypocenter and an increase in speed (2.5 km/s) at distances larger than 100 km from the hypocenter. Lay et al. (2011) explored the possibility of large near-trench slip during the great 2011 Tohoku earthquake by teleseismic P-waves inversion and estimated large slip (60 m) at shallow depth near the trench. Large slip near the trench was estimated using tsunami waveforms by previous studies (Fujii et al., 2011; Maeda et al., 2011; Saito et al., 2011). Total seismic moment estimates for the 2011 earthquake from previous studies using W-phase, teleseismic waveform, strong motion, and tsunami waveform are 3.9×10^{22} N m (Mw 9.0) (Ammon et al., 2011), 4.3×10^{22} N m (Mw 9.1) (Yoshida et al., 2011), 3.4×10^{22} N m (Mw 9.0) (Yoshida et al., 2011), and 3.8×10^{22} N m (Mw 9.0) (Fujii et al., 2011), respectively.

The 2011 Tohoku earthquake occurred within the Japan Trench subduction zone where the Pacific plate subducts beneath the Okhotsk plate. A large tsunami was generated by the 2011 Tohoku megathrust earthquake and devastated the coastal area along the north east coast of Honshu. The National Police Agency of Japan has confirmed casualties of about

16,000 deaths, 3,000 people missing, and 6,000 injured (http://www.npa.go.jp/archive/keibi/biki/higaijokyo_e.pdf). The tsunami was observed by tide gauges, pressure gauges, GPS buoys, and Deep-ocean Assessment and Reporting of Tsunamis (DART) buoys that are located offshore and across the Pacific Ocean. The 2011 Tohoku Earthquake Tsunami Joint Survey Group measured tsunami run-up at more than 5200 locations along the east coast of Tohoku area, maximum run-up heights greater than 10 m are distributed along 500 km of coast (Mori et al., 2012). Tsunami height exceeds 20 m at heads of V-shaped bays and apexes of peninsulas, and exceptional tsunami heights of over 35 m was measured at a small valley, Aneyoshi, on Omoe peninsula (Shimozono et al., 2012). Fritz et al., (2012) measured a maximum tsunami outflow currents of 11 m/s and an average water level increase of 1 m/minute within 12 minutes of flooding from survivor videos at Kesennuma Bay using LiDAR.

Old documents show that a large earthquake occurred off the coast of Sendai on 13 July 869. Tsunami deposit studies revealed the tsunami generated by the 869 Jogan earthquake inundated and damaged entire Sendai plain up to more than 4 km inland (Minoura et al., 2001; Namegaya et al., 2010). According to historical records, the 1611 Keicho Sanriku earthquake also generated large tsunami and inundated Sendai plain up to 4 km inland (Tsuji, 2003). To the north of the 2011 rupture area, two great earthquakes occurred off the coast of Sanriku; a thrust earthquake (Mw 8.5) that is identified as a tsunami earthquake event occurred in 1896 (Kanamori, 1972; Tanioka and Satake, 1996a); and an outer-rise earthquake (Mw 8.4) that occurred within the oceanic plate near the Japan Trench in 1933 (Kanamori, 1971). Both of the Sanriku earthquakes generated large tsunamis that devastated the Sanriku coastal area (Kanamori, 1972; Tanioka and Satake, 1996a). The 1978 (Mw 7.6) and the 2005 (Mw 7.2) Off-Miyagi earthquakes occurred within the rupture area of the 2011 earthquake (Yamanaka and Kikuchi, 2004; Miura et al., 2006).

A dense Global Positioning System (GPS) network of the Earth Observation Network (GEONET) on main islands of Japan that is maintained by Geospatial Information Authority of Japan (GSI) (Sagiya et al., 2000) detected coseismic and postseismic displacements due to the 2011 earthquake (Ozawa et al., 2011). Crustal movement monitoring at underwater reference stations off the east coast of Tohoku reveals that coseismic displacement there due to the earthquake is large up to 24 m of horizontal motion (Sato et al., 2011).

Previous studies indicated that large slip beneath a sedimentary wedge near the trench caused large horizontal movement of backstop and that generated large additional uplift of the sediment (Seno, 2000; Tanioka and Seno, 2001; Seno and Hirata, 2007). Those studies indicated that this additional uplift of sediment near a trench has large effect on tsunami generation. The uplift of sediments near the trench can be calculated from the horizontal movement of the backstop (Tanioka and Seno, 2001). Another tsunami generation mechanism that is associated with horizontal displacement of the sloping bathymetry near the trench was suggested by Tanioka and Satake (1996b).

The slip distribution of the 2011 earthquake inferred from GPS data at inland stations has a major slip region that is centered near the epicenter (Ozawa et al., 2011), whereas the slip distributions of the 2011 earthquake inferred from tsunami waveforms have the largest slip amounts at shallow depth near the trench (Fujii et al., 2011; Maeda et al., 2011; Saito et al., 2011). The tsunami waveforms and GPS data at these stations are important for developing a deeper understanding of the generation of a tsunami by a megathrust earthquake. The data at offshore stations provide strong constraints on the slip distribution of the earthquake. The tsunami waveforms observed at stations surrounding the source area and GPS data observed across Japan constrain the overall rupture area. In this paper we estimate the source model of the 2011 tsunami using tsunami waveforms, GPS data on main islands of Japan and seafloor crustal deformation data.

2. Observation data

2.1. Tsunami waveform data

To estimate slip distribution of the earthquake we use tsunami waveforms at 17 stations. These stations include 5 DART buoys in the Pacific Ocean (DART21401, DART21413, DART21418, DART21419 and DART52402), 2 tide gauges in Hokkaido Prefecture (Erimo and Mori), 1 tide gauge in Katsuura, Chiba Prefecture, 1 tide gauge in Ito, Shizuoka Prefecture, 2 bottom-pressure gauges off the coast of Tokachi (KPG1 and KPG2), 2 bottom-pressure gauges off the coast of Iwate Prefecture (TM1 and TM2), and 4 GPS buoys off the coast of Iwate, Miyagi, and Fukushima Prefectures (GPSB802, GPSB803, GPSB804 and GPSB806).

The National Oceanic and Atmospheric Administration (NOAA) operates the DART buoys. The Ministry of Land, Infrastructure, Transport, and Tourism (MLIT) operates the tide gauges in Mori, Hokkaido. The JMA operates the tide gauge in Erimo, Hokkaido. The GSI operates the tide gauges in Katsuura and Ito. The bottom pressure gauges of TM1 and TM2 are operated by University of Tokyo and Tohoku University, KPG1 and KPG2 are operated by the Japan Agency for Marine-Earth Science and Technology (JAMSTEC). MLIT and the Port and Airport Research Institute (PARI) operate the GPS buoys. The details of the stations are listed in **Table S1** and plotted on the map in **Fig. 2**.

These records include ocean tides, which should be removed to get the tsunami waveforms. The ocean tides are approximated by fitting a polynomial function, and are removed from the original records. The records from the 4 bottom-pressure sensors (KPG1, KPG2, TM1 and TM2) also contain high frequency waves; hence the tsunami waveforms are approximated by calculating the moving average of the record.

2.2. Crustal deformation data

Crustal deformation due to the 2011 Tohoku earthquake was observed by the GPS GEONET that is operated by the GSI. The Advanced Rapid Imaging and Analysis (ARIA) team at Jet Propulsion Laboratory (JPL) and California Institute of Technology (Caltech) estimated coseismic displacements due to the earthquake from 5 minutes interval of kinematic solutions of the GPS data. We use the coseismic displacements data (version 0.3, ftp://sideshow.jpl.nasa.gov/pub/usrs/ARIA/ARIA_coseismic_offsets.v0.3.table) estimated by the ARIA team at 1230 GPS stations in Japan to help estimate the slip distribution of the 2011 Tohoku earthquake.

Crustal deformation on the seafloor above the hypocenter of the 2011 earthquake has been measured using a technique that combines GPS and acoustic technologies at 5 seafloor reference points (KAMS, KAMN, MYGI, MYGW and FUKU) by the Japan Coast Guard (JCG). Displacements at the reference points due to mainshock, foreshocks and aftershocks of the 2011 earthquake until about 20 days after the mainshock are 5 to 24 m toward ESE and -0.8 to 3 m upward (Sato et al., 2011). Displacements due to effects other than the mainshock are estimated to be not larger than 1 m, therefore, the recorded displacements are considered as the coseismic displacements (Sato et al., 2011).

3. Joint inversion of tsunami waveforms and coseismic deformation data

3.1. Fault parameters

A ruptured plate interface is assumed to have a size with a length of 450 km and a width of 200 km by referring to aftershock distribution (**Fig. 1**). Then the plate interface is divided into 45 subfaults with length and width of 50 km and 40 km, respectively. Strike for each subfault is assumed to be 202°, dip angles of 5°, 10°, 15°, 18° and 20° are used for the subfaults at depth of 1.0 km, 4.5 km, 11.5 km, 21.8 km and 34.2 km, respectively (**Fig. 1**).

147 Rake angles of 45° and 135° are used for each subfault to estimate the slip direction of each
148 subfault (within the range between 45° and 135°).

149 The initial sea surface deformation is assumed to be the same as the ocean bottom
150 deformation if the spatial wavelength of the ocean bottom deformation is much larger than
151 the ocean depth (Satake, 2002). This assumption cannot be applied to obtain sea surface
152 deformation from the ocean bottom deformation that is induced by faulting of a very shallow
153 fault near a trench, because the deformation near the trench has steep slope with spatial
154 wavelength that is smaller than ocean depth. Therefore, the initial sea surface deformation for
155 subfaults near the trench (A and B subfaults) (**Fig. 1**) is computed from the coseismic vertical
156 deformation on the ocean bottom using Kajiura (1963) formula. For the other subfaults, it is
157 assumed to be equal to the coseismic vertical deformation. The coseismic horizontal and
158 vertical deformations on the ocean bottom are computed for each subfault with unit amount
159 of slip using Okada (1985) formula.

160 ***3.2. Tsunami numerical simulation***

161 The bathymetry data sets used for tsunami simulation are based upon the General
162 Bathymetric Chart of the Oceans (GEBCO) 30 arc-second data set and the Japan
163 Hydrographic Association's M7001 and M7006 bathymetric contour data sets. The
164 computation area ranges from 130° to 160° E and from 10° to 50° N. We use different grid
165 systems with grid sizes of 90 arc-seconds, 30 arc-seconds, and 10 arc-seconds to compute the
166 tsunami. The finest grids are used for the coastal area around the Erimo, Mori, Katsuura, and
167 Ito tide gauge stations.

168 Synthetic tsunami waveforms generated from all subfaults at the stations were
169 numerically computed by solving the linear shallow water equations with spherical
170 coordinate system (Johnson, 1998). We used a tsunami model that has been developed and

used in tsunami waveform inversion studies (i.e. Fujii and Satake, 2008; Tanioka et al., 2008; Gusman et al., 2010; Fujii et al., 2011). Tsunami in the deep ocean is not affected by coastal effects and simulation of the tsunami using the linear shallow water equations is widely accepted (Synolakis et al., 2008). While the nonlinearity becomes important around coastal tide gauge stations, Fujii et al. (2011) confirmed by comparing the nonlinear and linear computations that they produce similar arrival times and initial slopes. The sea level observation instruments used different sampling rates, so the tsunami waveforms are resampled at 15 seconds interval and the synthetic tsunami waveforms are also resampled at 15 seconds interval.

3.3. Joint inversion

We estimate a slip distribution by a joint inversion using the tsunami waveforms and crustal deformation data. A green's function for the joint inversion is made from the synthetic of tsunami waveforms and crustal deformation using the fault parameters. The number of tsunami waveforms data points that we used is 2989, while the number of crustal deformation data points at the 1235 stations is 3705.

We used non-negative least square method (Lawson and Hanson, 1974) and include a spatial smoothness constraint to estimate the slip distribution of the earthquake. The optimal value of smoothing factor was selected to minimize Akaike's Bayesian information criterion (ABIC) (Akaike, 1980). For more details of our inversion method, see Gusman et al. (2010). A "delete-half" Jackknife resample is extracted from the original data by deleting half the number of data points. The standard error of the slip distribution is calculated using 50 models that are estimated from the "delete-half" Jackknife resamples (Tichelaar and Ruff, 1989).

4. Results

195 The maximum slip amount is estimated to be 44 m and the major slip region is
196 located up-dip of the hypocenter with dimensions of roughly 300 km length and 160 km
197 width (**Fig. 3a**). The earthquake ruptured the plate interface from the hypocenter all the way
198 to the trench with large slip amount, about 41 m, near the trench. These results are consistent
199 with results from inversion analysis based on dispersive tsunami simulation by Saito et al.
200 (2011). The seismic moment calculated from the slip distribution is 5.5×10^{22} N m (Mw 9.1)
201 by assuming the rigidity of 4×10^{10} N m^{-2}. The estimated average rake angle from the slip
202 distribution is 88° (**Fig. 4a**), which is equal to the rake angle at the centroid (GCMT). The
203 slip distribution generated sea surface deformation with a maximum water level of about 9 m
204 above mean sea level (**Fig. 3c**).

205 The calculated horizontal and vertical displacements at GPS stations and at seafloor
206 reference points resemble the observations. Comparisons between the calculated and the
207 observed horizontal and vertical displacements are shown in **Fig. 5a**. We compare the
208 simulated tsunami waveforms from the estimated slip distribution with the observed tsunami
209 waveforms at sea level observation stations in **Fig. 6**. Overall, observed tsunami waveforms
210 are well explained by simulated tsunami waveforms.

211 **5. Discussion**

212 The main difference between the slip distributions of the 2011 earthquake estimated
213 from GPS data (i.e. Ozawa et al., 2011) and those estimated from tsunami waveforms (i.e.
214 Fujii et al., 2011; Maeda et al., 2011; Saito et al., 2011) is the location of the largest slip
215 amount. The slip distribution estimated from GPS data concentrated near the epicenter
216 whereas that estimated from tsunami waveforms has large slip near the trench. By using
217 tsunami waveforms, GPS data and seafloor crustal deformation data in a joint inversion, a
218 more accurate slip distribution of the 2011 earthquake can be estimated. In this study, the slip

219 distribution of the 2011 earthquake estimated from tsunami waveforms and crustal
220 deformation data has large slip near the trench similar to those estimated by previous studies
221 (Fujii et al., 2011; Maeda et al., 2011; Saito et al., 2011), and the slip distribution can explain
222 well the tsunami waveforms and crustal deformation data.

223 Because Tanioka and Seno (2001) suggested that the additional uplift along the
224 unconsolidated sedimentary wedge near the trench generated the additional tsunami for the
225 1896 Sanriku tsunami, we also need to test that the observed tsunami waveforms can be
226 explained by the additional uplift near the trench. In this study, the calculation of the
227 additional uplift is following the Model A in Tanioka and Seno (2001). The uplift of the
228 sediments, u_s, is represented by $u_s = u_h \tan\theta$ where u_h is the horizontal movement due to
229 earthquake, and θ is the dip angle of the slope. A seismic profile after the 2011 earthquake
230 provided by JAMSTEC shows a large bathymetric change near the trench that has a width of
231 1.5 km. To calculate additional uplift, we assume that the dip angle of the backstop slope (θ)
232 is 50°, which is the same as that of Tanioka and Seno (2001), and the width of uplift area is
233 1.5 km. The horizontal movement (u_h) is computed for each subfault "A" with unit amount of
234 slip using Okada (1985) formula. The sea surface deformation of the additional uplift is
235 calculated by the Kajiura (1963) formula because the width of the additional uplift is 1.5 km,
236 which is smaller than the ocean depth. Then a slip distribution is estimated by joint inversion
237 using green's function that is made from both faulting and additional uplift. .

238 The seismic moment calculated from the estimated slip distribution (**Fig. 3b**) is $5.1 \times$
239 10^{22} N m (Mw 9.1) by assuming the rigidity of 4×10^{10} N m^{-2}. The inferred slip distribution
240 and inferred additional uplift generated initial sea surface deformation with a distinctive short
241 wavelength and high peak (11 m) near the trench (**Fig. 3d**). The calculated horizontal and
242 vertical displacements are consistent with the observations (**Fig. 5b)**. Comparison between
243 the observed and simulated tsunami waveforms from the source model with additional uplift

244 is shown in **Fig. 7**. Observed tsunami waveforms and crustal deformation data are explained
245 well by the result from the source model with additional uplift.

246 To evaluate the fitness between simulated and observed data from both source models,
247 the root mean square (RMS) of the residual between simulated and observed data from each
248 of source model is calculated. The RMS for the tsunami waveforms and crustal deformation
249 from the results of the source model with additional uplift are 31.1 cm and 11.9 cm,
250 respectively. These are smaller than those calculated from the results of the source model
251 without additional uplift, which are 33.3 cm for tsunami waveforms and 12.0 cm for crustal
252 deformation. Standard error of each slip distribution is calculated by using Jackknife
253 technique. The maximum error for the slip distribution without additional uplift is ± 6.1 m,
254 which is relatively small (**Fig. 4a**). The slip distribution with additional uplift is improved
255 with smaller error than that for the slip distribution without additional uplift (**Fig. 4b**). These
256 suggest that the additional uplift as the same as the 1896 Sanriku tsunami earthquake might
257 occur during the 2011 great Tohoku earthquake because the 2011 Tohoku earthquake also
258 ruptured the plate interface near the Japan Trench.

259 To analyze the effect of additional uplift near the trench on tsunami generation, the
260 tsunami waveforms generated by the coseismic vertical deformation and those generated by
261 the additional uplift due to the coseismic horizontal deformation are simulated separately.
262 Then we integrate the first cycle of the generated tsunami waveforms at each station. The
263 tsunami waveforms generated from the additional uplift at all stations range from 10 % to
264 30 % of the combined tsunami waveforms from both coseismic vertical deformation and
265 additional uplift.

266 The seafloor crustal deformation data strongly constrains the slip distribution because
267 the locations of the stations are right above the plate interface. Because we use crustal

deformation data in addition to tsunami waveforms to estimate a slip distribution, the fit to tsunami waveforms from our result is slightly worse than those from results that used only tsunami waveforms (e.g. Fujii et al., 2011; Saito et al., 2011). The misfit from our result is more apparent at DART21418, whereas slip distributions estimated by tsunami inversion studies (e.g. Fujii et al., 2011; Saito et al., 2011) can explain well the tsunami waveforms at DART21418. Saito et al. (2011) also suggest that dispersive tsunami is recorded at DART21418.

Ito et al. (2011) observed seafloor horizontal and vertical displacements at three stations (GJT3, TJT1, and TJT2) near the Japan Trench, and estimated a localized slip amount of 80 m near the trench to explain the observed displacements. The calculated vertical displacements of around 5.5 and 4.5 m from our slip distributions are very close to the observations of 5 (± 2) m and 5 (± 0.5) m at GTJ3 and TJT1, respectively. While the calculated horizontal displacements of 30-34 m from our slip distributions are smaller than the observations of 31 ± 1 m, 58 ± 20 m, and 74 ± 20 m at the three stations. The discrepancies may be explained by the difference of dip angle used in the two studies (i.e. this study dip is 5° and in Ito et al. (2011) dip is 3°). The misfits may be reduced by further study of source models for this event that use a smaller subfault size and synthetic tsunami waveforms solved with dispersive tsunami equations.

6. Conclusions

In this study, joint inversion is performed using tsunami waveforms, GPS data and seafloor deformation data to study the source model of the 2011 earthquake. The earthquake ruptured the plate interface from the hypocenter all the way to the trench with large slip amounts up to 41 m on the shallowest subfaults. Total seismic moment calculated from

292 estimated slip distributions with and without additional uplift are 5.1 and 5.5 × 10^{22} N m (Mw
293 9.1), respectively, which are consistent with that estimated by GCMT (5.3 × 10^{22} N m).

294 The large maximum slip is strongly constrained by the seafloor crustal deformation
295 data near the epicenter. The tsunami waveforms data at offshore stations near the source area
296 strongly constrain the generated initial sea surface deformation. These emphasize the
297 importance of seafloor monitoring and offshore sea level observation to accurately estimate
298 the slip distribution near the trench of interplate earthquakes in the subduction zone.

299 We indicate that not only coseismic vertical deformation but also additional uplift
300 near the trench as suggested for the 1896 Sanriku tsunami earthquake may contribute the
301 large tsunami near the seismic source of the 2011 Tohoku earthquake.

302 **Acknowledgements**

303 GPS buoy data are provided by MILT and PARI. KPG1 and KPG2 pressure gauge
304 data are provided by JAMSTEC. TM1 and TM2 pressure gauge data are provided by Tohoku
305 University and University of Tokyo. DART buoy data are downloaded from NOAA's
306 website. Erimo and Mori tide gauge data are provided by JMA. Katsuura and Ito tide gauge
307 data are downloaded from GSI's website. Preliminary GPS time series provided by the ARIA
308 team at JPL and Caltech, all original GEONET RINEX data provided to Caltech by the
309 Geospatial Information Authority (GSI) of Japan. Seafloor crustal deformation data are
310 provided by Japan Coast Guard. We thank Peter M. Shearer and two anonymous reviewers
311 for their constructive comments.

312

313 **References**

314 Akaike, H., 1980. Likelihood and the Bayes procedure, in: J. M. Bernando et al. (Eds.),
315 Bayesian Statistics. Univ. Press, Valencia, Spain, pp. 143-166.

316 Ammon, C. J., Lay, T., Kanamori, H., Cleveland, M., 2011. A rupture model of the 2011off
317 the Pacific coast of Tohoku earthquake. Earth Planets Space 63, 693-696.

318 Fritz, H. M., Phillips, D. A., Okayasu, A., Shimozono, T., Liu, H., Mohammed, F., Skanavis,
319 V., Synolakis, C.E., Takahashi, T. (2012). The 2011 Japan tsunami current velocity
320 measurements from survivor videos at Kesennuma Bay using LiDAR, Geophys. Res. Lett.,
321 39, L00G23, doi:10.1029/2011GL050686.

322 Fujii, Y., and Satake, K., 2008, Tsunami sources of the November 2006 and January 2007
323 great Kuril earthquakes, Bull. Seismol. Soc. Am. 98, 1559-1571.

324 Fujii, Y., Satake, K., Sakai, S-I., Shinohara, M., Kanazawa, T., 2011. Tsunami source of the
325 2011 off the Pacific coast of Tohoku, Japan earthquake. Earth Planets Space 63, 815-820.

326 Gusman, A. R., Tanioka, Y., Kobayashi, T., Latief, H., Pandoe, W., 2010. Slip distribution of
327 the 2007 Bengkulu earthquake inferred from tsunami waveforms and InSAR data. J. Geophys.
328 Res. 115, B12316, doi:10.1029/2010JB007565.

329 Ito, Y., Tsuji, T., Osada, Y., Kido, M., Inazu, D., Hayashi, Y., Tsushima, H., Hino, R., and
330 Fujimoto, H., 2011. Frontal wedge deformation near the source region of the 2011 Tohoku-
331 Oki earthquake. Geoph. Res. Lett. 38, L00G05, doi:10.1029/2011GL048355.

332 Johnson, J. M., 1998. Heterogeneous coupling along Alaska-Aleutians as inferred from
333 tsunami, seismic, and geodetic inversions. Adv. Geophys. 39, 1-116.

334 Kajiura, K., 1963. The leading wave of a tsunami. Bulletin of the Earthquake Research
335 Institute 41, 535-571.

336 Kanamori, H., 1971. Seismological evidence for a lithospheric normal faulting – the Sanriku
337 earthquake of 1933. Phys. Earth Planet. Inter. 4, 289-300.

338 Kanamori, H., 1972. Mechanism of tsunami earthquakes. Phys. Earth Planet. Inter. 6, 346-
339 359.

340 Lay, T., Ammon, C. J., Kanamori, H., Xue, L., Kim, M. J., 2011. Possible large near-trench
341 slip during the 2011 Mw 9.0 off the Pacific coast of Tohoku earthquake. Earth Planets Space
342 63, 687-692.

343 Lawson, C. L., Hanson, B. J., 1974. Solving least squares problems, Prentice Hall Inc.,
344 Englewood Cliffs, New Jersey, US.

345 Maeda T., Furumura, T., Sakai, S., Shinohara, M., 2011. Significant tsunami observed at the
346 ocean-bottom pressure gauges at 2011 the Pacific Coast of Tohoku Earthquake. Earth Planets
347 Space 63, 803-808.

348 Minoura, K., Imamura, F., Sugawara, D., Kono, Y., Iwashita, T., 2001. The 869 Jogan
349 tsunami deposit and recurrence interval of large-scale tsunami on the Pacific coast of
350 northeast Japan. Journal of Natural Disaster Science 23-2, 83-88.

351 Miura, S., Iinuma, T., Yui, S., Uchida, N., Sato, T., Tachibana, K., Hasegawa A., 2006. Co-
352 and postseismic slip associated with the 2005 Miyagi-oki earthquake (M7.2) as inferred from
353 GPS data. Earth Planets Space 58, 1567-1572.

354 Mori, N., Takahashi, T. and the 2011 Tohoku Earthquake Tsunami Joint Survey Group
355 (2012). Nationwide post event survey and analysis of the 2011 Tohoku earthquake tsunami.
356 Coastal Eng. J., 54(1), 1250001, doi: 10.1142/S0578563412500015.

357 Namegaya, Y., Satake, K., Yamaki, S., 2010. Numerical simulation of the AD 896 Jogan
358 tsunami in Ishinomaki and Sendai plains and Ukedo river-mouth lowland. Annual Report on
359 Active Fault and Paleoearthquake Researches 10, 1-21. (in Japanese)

360 Okada, Y., 1985. Surface deformation due to shear and tensile faults in half-space. Bull.
361 Seism. Soc. Am. 75-4, 1135-1154.

362 Ozawa S., Nishimura, T., Suito, H., Kobayashi, T., Tobita, M., Imakiire, T., 2011. Coseismic
363 and postseismic slip of the 2011 magnitude-9 Tohoku-Oki earthquake, Nature 475, 373-376,
364 doi:10.1038/nature10227.

365 Sagiya, T., Miyazaki, S., Tada, T., 2000. Continuous GPS array and present-day crustal
366 deformation of Japan, Pure Appl. Geophys. 157, 2303-2322.

367 Saito, T., Ito, Y., Inazu, D., and Hino, R., 2011. Tsunami source of the 2011 Tohoku-Oki
368 earthquake, Japan: Inversion analysis based on dispersive tsunami simulations, Geophys. Res.
369 Lett. 38, L00G19, doi:10.1029/2011GL049089.

370 Satake, K., 2002. Tsunamis, in: W.H.K. Lee et al. (Eds.), International Handbook of
371 Earthquake and Engineering Seismology 81A. Academic Press, China, pp. 437-451.

372 Sato, M., Ishikawa, T., Ujihara, N., Yoshida, S., Fujita, M., Mochizuki, M., Asada, A., 2011.
373 Displacement above the hypocenter of the 2011 Tohoku earthquake. Science, 1-2,
374 doi:10.1126/science.1207401.

375 Seno, T., 2000. The 21 September, 1999 Chichi earthquake in Taiwan: implications for
376 tsunami earthquakes. Terr. Atmos. Ocean Sci. 11, 701-708.

377 Seno, T.,Hirata, K., 2007. Did the 2004 Sumatra-Andaman earthquake involve a component
378 of tsunami earthquakes? Bull. Seism. Soc. Am. 97-1A, S296-S306, doi:10.1785/0120050615.

379 Shimozono, T., Sato, S., Okayasu, A., Tajima, Y., Fritz, H.M., Liu, H., Takagawa, T. (2012).
380 Propagation and Inundation Characteristics of the 2011 Tohoku Tsunami on the Central
381 Sanriku Coast, Coastal Eng. J., 54(1), 1250004, doi:10.1142/S0578563412500040.

382 Synolakis, C. E., Bernard, E. N., Titov, V. V., Kanoglu, U., Gonzalez, F. I., 2008. Validation
383 and verification of tsunami numerical models. Pure Appl. Geophys. 165, 2197-2228,
384 doi:10.1007/s00024-004-0427-y.

385 Tanioka, Y., Satake, K., 1996a. Fault parameters of the 1896 Sanriku tsunami earthquake
386 estimated from tsunami numerical modeling. Geophys. Res. Lett. 23-13, 1549-1552.

387 Tanioka, Y., Satake, K., 1996b. Tsunami generation by horizontal displacement of ocean
388 bottom, Geophys. Res. Lett. 23 (8), 861-864, doi:10.1029/96GL00736.

389 Tanioka, Y., Seno, T., 2001. Sediment effect on tsunami generation of the 1896 Sanriku
390 tsunami earthquake. Geophys. Res. Lett. 28-17, 3389-3392.

391 Tanioka, Y., Hasegawa, Y., and Kuwayama, T., 2008, Tsunami waveform analyses of the
392 2006 underthrust and 2007 outer-rise Kurile earthquakes, Advances in Geosciences 14, 129-
393 134.

394 Tichelarr, B. W., and Ruff, L. J., 1989. How good are our best models? Jackknifing,
395 bootstrapping, and earthquake depth, Eos Trans. AGU. 70, 593, 605-606.

396 Tsuji, T., Ito, Y., Kido, M., Osada, Y., Fujimoto, H., Ashi, J., Kinoshita, M., and Matsuoka,
397 T., 2011. Potential tsunamigenic faults of the 2011 off the Pacific coast of Tohoku earthquake.
398 Earth Planets and Space 63, 831-834.

399 Tsuji, Y., 2003. Special characteristic of the 1611 Keichou Sanriku tsunami. Chikyu Monthly
400 25-5, 374-381. (in Japanese).

401 Yamanaka, Y., Kikuchi, M., 2004. Asperity map along the subduction zone in northeastern
402 Japan inferred from regional seismic data. J. Geophys. Res. 109, B07307,
403 doi:10.1029/2003JB002683.

404 Yoshida, Y., Ueno, H., Muto, D., Aoki, S., 2011. Source process of the 2011 off the Pacific
405 Coast of Tohoku earthquake with the combination of teleseismic and strong motion data.
406 Earth Planets Space 58, 1-5.

407

408 **Figures**

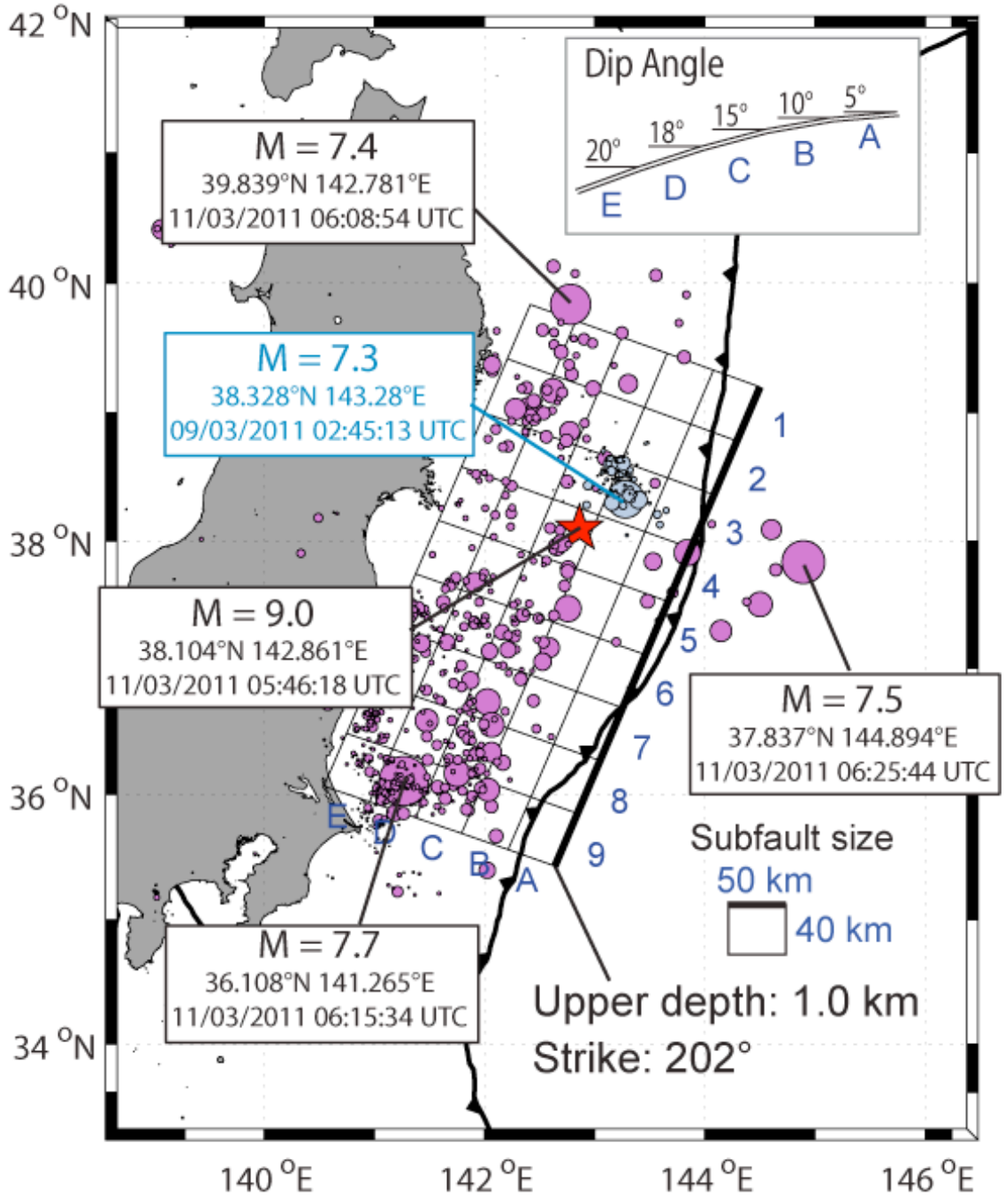

409

410 Fig. 1. Map of the 2011 Tohoku earthquake. Red star represents the epicenter of the

411 mainshock, gray circles represent foreshocks and purple circles represent aftershocks and

412 extensional faulting events in the outer-rise.

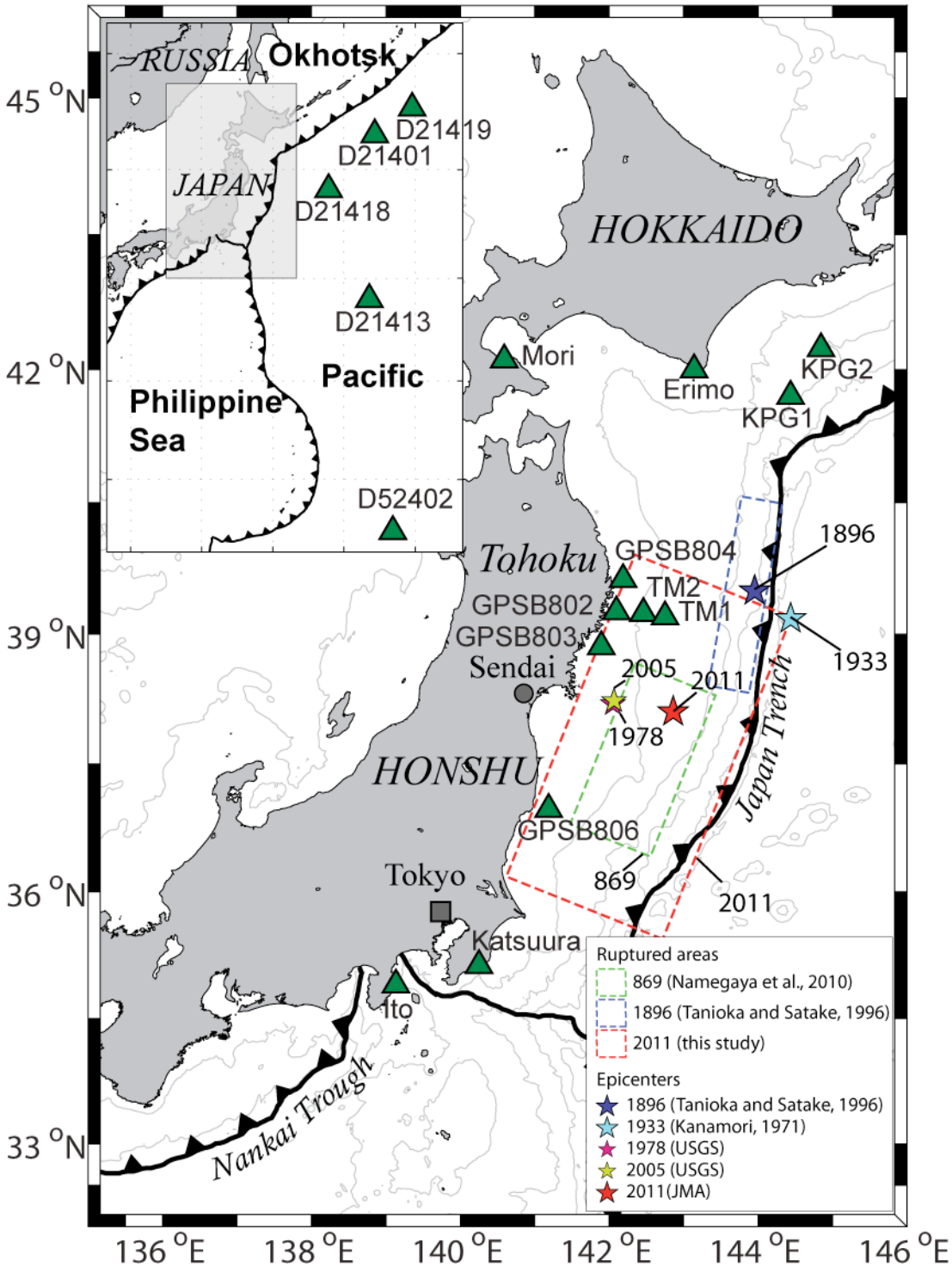

413

414 Fig. 2. Map of sea level observation stations (green triangles). Stars represent epicenters and

415 rectangles represent ruptured areas.

416

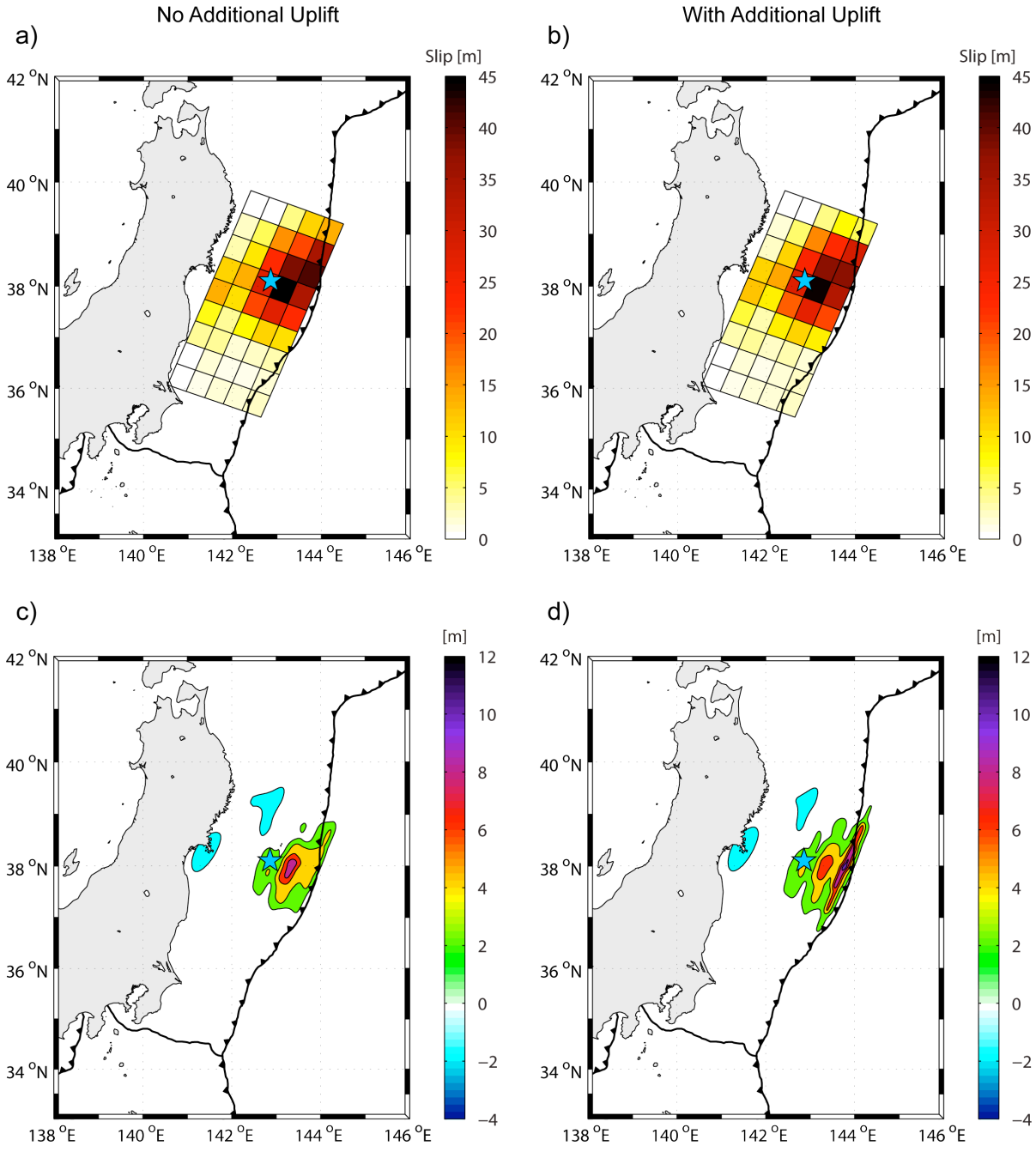

417

418 Fig. 3. a) Slip distribution of the 2011 Tohoku earthquake estimated from tsunami waveforms
419 and crustal deformation data and b) estimated slip distribution of the 2011 Tohoku
420 earthquake when the green's function is constructed from both faulting and additional uplift.
421 c) Sea surface deformation generated from the slip distribution of **Fig. 3a**. d) Sea surface
422 deformation generated from the slip distribution of **Fig. 3b** and the inferred additional uplift.
423 Light blue star represents the epicenter of the earthquake.

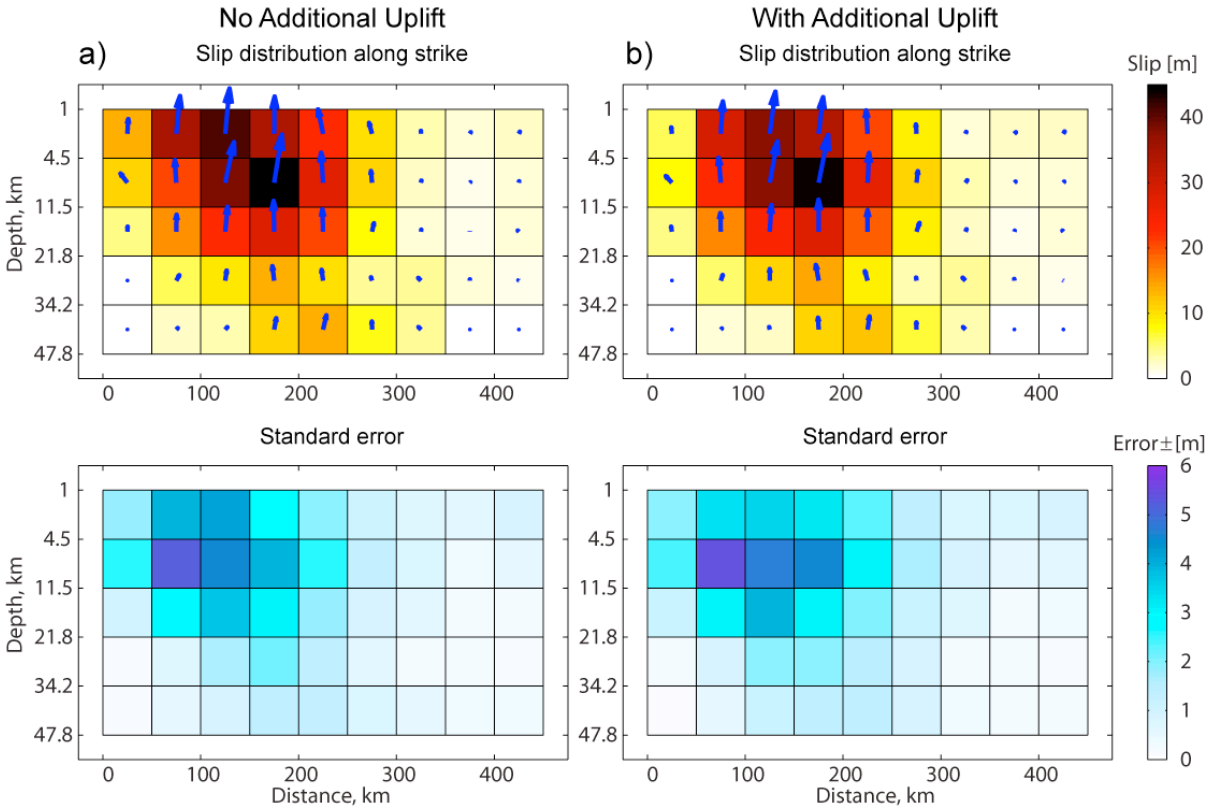

424

425 Fig. 4. Slip distribution and its "delete-half" Jackknife standard deviation (standard error). a)
426 Slip distribution along strike of the 2011 Tohoku earthquake estimated from tsunami
427 waveforms and crustal deformation data. b) Estimated slip distribution along strike of the
428 2011 Tohoku earthquake when the green's function is constructed from both faulting and
429 additional uplift. Blue arrow represents the inferred rake angle of each subfault.

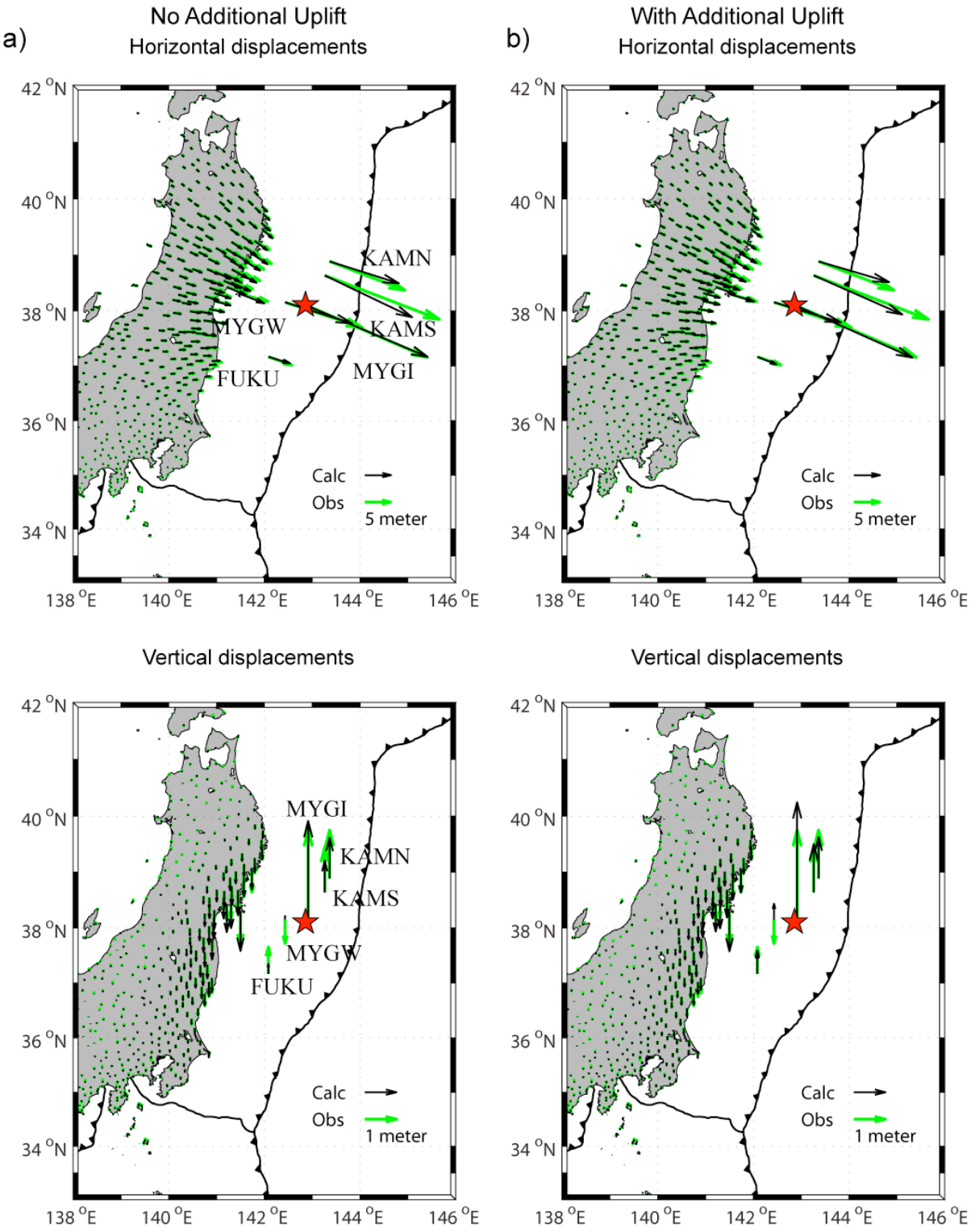

Fig. 5. Comparison between observed (green arrows) and calculated (black arrows) coseismic displacements. a) Horizontal and vertical displacements calculated from the slip distribution of **Fig. 3a**. b) Horizontal and vertical displacements calculated from the slip distribution of **Fig. 3b**.

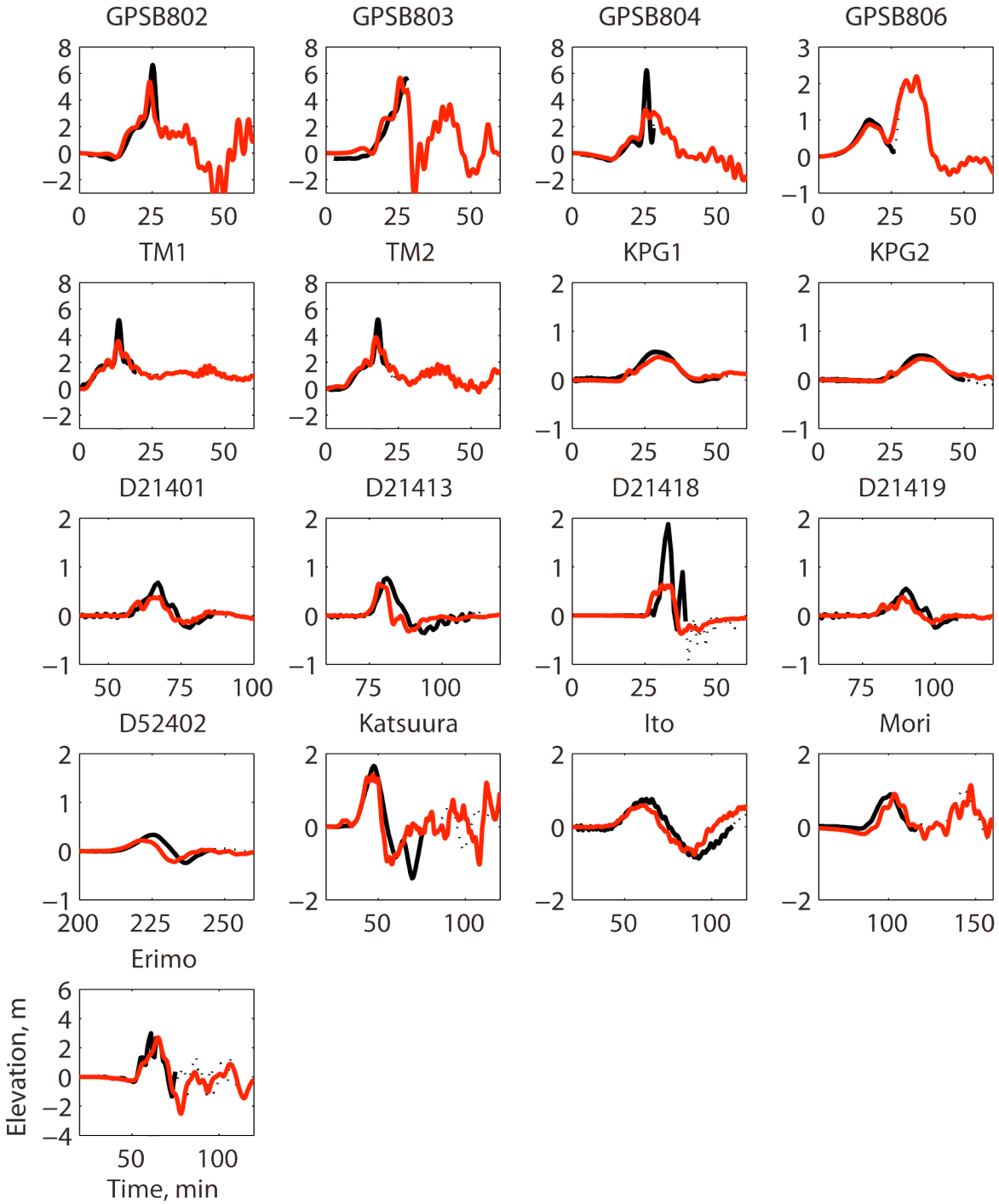

435

436 Fig. 6. Observed and simulated tsunami waveforms from the slip distribution of **Fig. 3a**. Red
437 lines represent the simulated tsunami waveforms, black lines represent the observed tsunami
438 waveforms that are used in the inversion, and black dashed lines are the observed tsunami
439 waveforms.

440

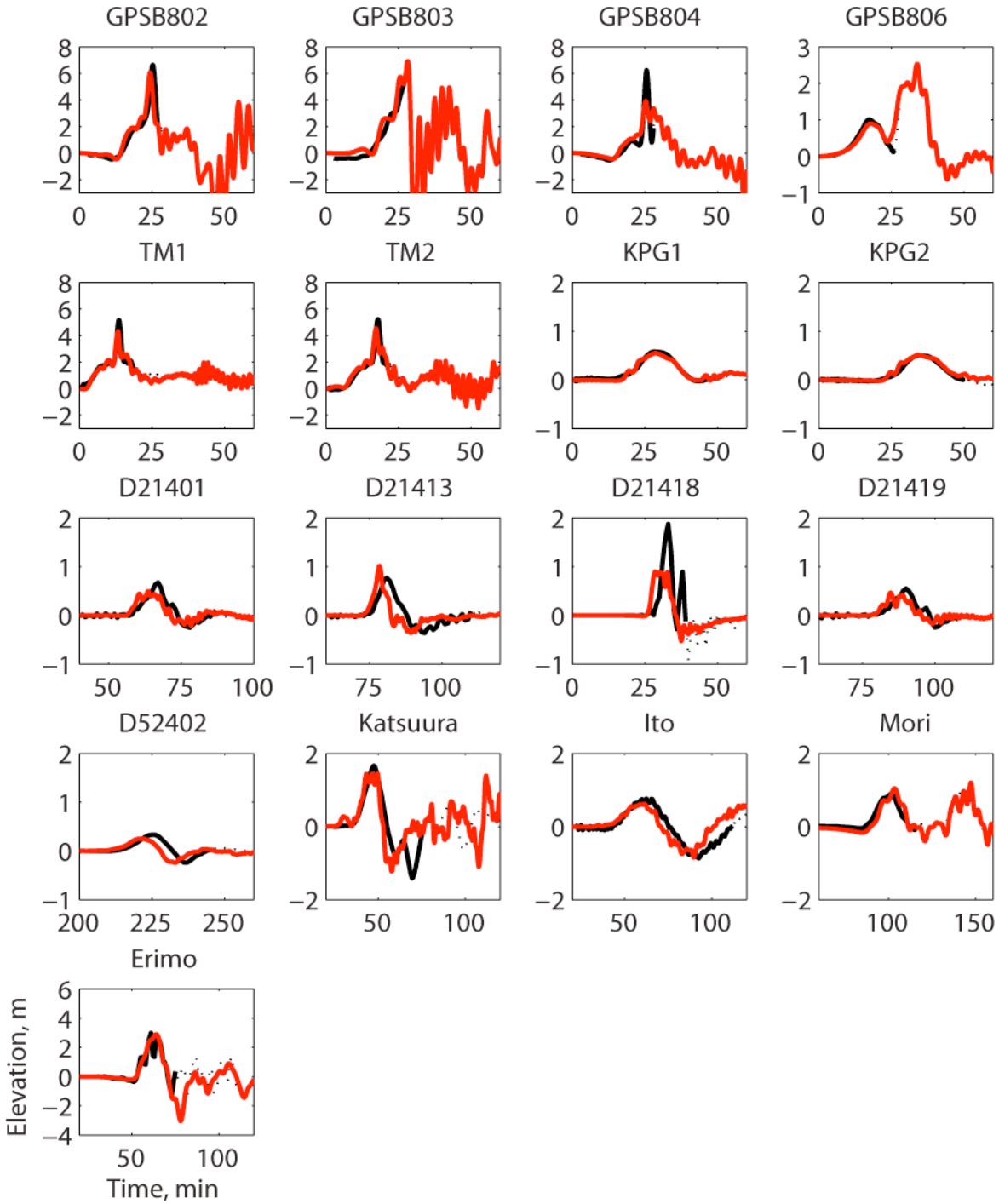

441

442 Fig. 7. Observed and simulated tsunami waveforms from source model with the additional
443 uplift. Red lines represent the simulated tsunami waveforms, black lines represent the
444 observed tsunami waveforms that are used in the inversion, and black dashed lines are the
445 observed tsunami waveforms.

446

447 **Table**

448 Table S1. List of bottom-pressure, GPS buoy, and tide gauge stations.

No	Name	Longitude (°E)	Latitude (°N)	Type	Authority	Maximum amplitude (cm)	Arrival time in minutes after time origin
1.	DART 21401	152.583	42.617	Bottom-pressure	RFERHRI and NOAA	67	67
2.	DART 21413	152.123	30.528	Bottom-pressure	NOAA	77	81
3.	DART 21418	148.698	38.718	Bottom-pressure	NOAA	187	33
4.	DART 21419	155.735	44.455	Bottom-pressure	NOAA	55	90
5.	DART 52402	154.111	11.882	Bottom-pressure	NOAA	32	224
6.	Erimo	143.142	42.000	Tide gauge	JMA	298	61
7.	Mori	140.591	42.112	Tide gauge	MLIT and PARI	88	101
8.	Katsuura	140.250	35.133	Tide gauge	GSI	166	47.5
9.	Ito	139.133	34.900	Tide gauge	GSI	76	62.5
10.	KPG1	144.438	41.704	Bottom-pressure	JAMSTEC	58	28.3
11.	KPG2	144.845	42.236	Bottom-pressure	JAMSTEC	50	35.5
12.	TM1	142.750	39.200	Bottom-pressure	Tohoku Univ and Univ. of Tokyo	516	13.6
13.	TM2	142.460	39.240	Bottom-pressure	Tohoku Univ and	521	17.9

					Univ. of Tokyo		
14.	GPSB802	142.097	39.259	GPS buoy	MLIT and PARI	664	25.2
15.	GPSB804	142.187	39.627	GPS buoy	MLIT and PARI	623	25.6
16.	GPSB803	141.894	38.858	GPS buoy	MLIT and PARI	563	27.5
17	GPSB806	141,1856	36.9714	GPS buoy	MLIT and PARI	100	17.45

449 GSI: Geospatial Information Authority of Japan

450 JAMSTEC: Japan Agency for Marine-Earth Science and Technology

451 JMA: Japan Meteorological Agency

452 MLIT: Ministry of Land, Infrastructure, Transport, and Tourism

453 NOAA: National Oceanic and Atmospheric Administration

454 PARI: Port and Airport Research Institute

455